Adsorption (2009) 15: 99–113
DOI 10.1007/s10450-009-9158-9

# Adsorption potential distributions for carbons having defined pore structure—GCMC simulations of the effect of heterogeneity

**Piotr A. Gauden · Artur P. Terzyk · Sylwester Furmaniak · Piotr Kowalczyk**

Published online: 23 March 2009


**Abstract** Adsorption Potential Distribution (APD) is one of the most important and widely propagated by Jaroniec and co-workers method since it is modeless. Using the GCMC simulation of Ar adsorption in pores with well defined geometry (slit-like, cylindrical, hexagonal and quadratic) we study the effect of heterogeneity on the APDs. The heterogeneity is introduced by controlled removal of carbon atoms from the first internal layer of an adsorbent. Since defects are introduced for pores having different initial geometries it is possible to study the systematic changes in the APD curves.

**Keywords** Adsorption · GCMC · Adsorption potential distribution · Activated carbon · Carbon nanotubes · Slit-like pores · Heterogeneity

**Notations**

| | |
|---|---|
| $a$ | adsorption |
| $a_{max}$ | maximal adsorption |
| $A_{pot}$ | adsorption potential |
| $A_{potmax}$ | adsorption potential maximum |
| APD | adsorption potential distribution |
| $D_{cyl}$ | the diameter of cylindrical pore |
| $d_{CC}$ | the length of C-C bond |
| $\Delta$ | interlayer spacing |
| $\varepsilon$ | the depth of the potential well |
| $F$ | the four parameter hypergeometric function |
| GCMC | grand canonical Monte Carlo |
| $H_{slit}$ | the width of the slit-like pore |
| $H_{quad}$ | the width of the quadratic pore |
| $H_{hex}$ | the width of the hexagonal pore |
| $I_{potmax}$ | maximal intensity of the adsorption potential |
| $k_B$ | Boltzmann constant |
| $L_z$ | the length of the simulation box in the $z$ direction |
| $M$ | the number of carbon atoms forming the internal layer |
| $p$ | pressure |
| $p_s$ | saturation vapour pressure |
| $R$ | the tube diameter, |
| $R_g$ | gas constant |
| $R^*$ | the reduced radius of the nanotube |
| $R_{cut}$ | the radius of the cutting sphere |
| $r$ | distance |
| $r_{cut}$ | cut-off limit for Lennard–Jones potential |
| $\rho_s$ | the density of carbon atoms in the wall |
| $\sigma$ | collision diameter |
| $U$ | potential energy |
| $w_s$ | the diameter of the layer. |

**Electronic supplementary material** The online version of this article (doi:http://dx.doi.org/10.1007/s10450-009-9158-9) contains supplementary material, which is available to authorized users.

P.A. Gauden · A.P. Terzyk (✉) · S. Furmaniak
Department of Chemistry, Physicochemistry of Carbon Materials Research Group, N. Copernicus University, Gagarin St. 7, 87-100 Toruń, Poland
e-mail: aterzyk@chem.uni.torun.pl
url: http://www.chem.uni.torun.pl/~aterzyk/

P. Kowalczyk
Applied Physics, RMIT University, GPO Box 2476V, Victoria 3001, Australia

## 1 Introduction

Adsorption potential distribution (APD) concept was introduced by Timofeev (1974). He noticed that the conversion of benzene adsorption isotherms (measured on two samples of coals) into the related APDs, can be a simple indicator

of porosity. In this way he postulated that there is the relation between pore diameter and the location of maxima on the APDs curves. As it was pointed out by professor Jaroniec in many privet conversations, the major advantage of the APD curve is its modeless, i.e. it is calculated only by simple differentiation of an adsorption isotherm. Due to progress in measurements, adsorption isotherms are now determined with very high precision and from extremely small pressure values ($\sim 10^{-6}$ $p/p_s$ for $N_2$ (77 K)). Thus, the creation of layers can be observed and all nuances of adsorption isotherms are reflected in results. Therefore, the careful examination of the APD is now one of the simplest methods for studying the mechanisms of adsorption and the structure of different adsorbents, as it was shown in many papers (Choma and Jaroniec 1997, 2001; Darmstadt and Roy 2001; Gil 1998; Jaroniec and Choma 1986, 1997; Korili and Gil 2001; Kruk et al. 1998, 1999a; McEnaney et al. 1987; Puziy 1995).

On the other hand, it is well known that some problems can occur with APD curves, especially if adsorption of polar molecules is studied. Moreover since we use differentiation the APD idea can be applied only for some ranges of adsorption isotherms.

One of the most interesting study, showing how strong from past up to presence is the evolution of Timofeev's concept was published by Kruk et al. (1999b). In this study by careful examination of adsorption isotherms measured for the series of synthetic activated carbons (having progressively changed porosity) mentioned authors discussed the relation between the shape and location of the peaks on the APDs curves and adsorption mechanism. Moreover, the relations between the average micropore size and the adsorption potential of the maximum of the monolayer formation peak, and the average micropore size and the adsorption potential of the maximum of the secondary micropore filling peak were also given. The recovering of those relations by molecular simulations of Ar adsorption on carbons having the fullerene-like structures was presented recently (Terzyk et al. 2007).

In the current study we show the analysis of the APDs on molecular level. Since to propose (from experimental data) the relations obtained in Kruk et al. (1999b) it was necessary to assume the ideal geometry of the adsorption space (slit-like porosity was assumed by Kruk et al.) it is not easy (basing on the experimental data) to study and evaluate the influence of heterogeneity of pore walls on the shape and properties of APD curves. Fortunately, this problem can be solved using molecular simulations since the structure of a solid, and the heterogeneity of pore walls, are known. Therefore, in this study, assuming ideal slit-like, cylindrical, hexagonal and quadratic pores and pores with defects we try to find answers to the questions how the geometry of adsorption space and the heterogeneity of the walls influence on the properties of the APD curves.

## 2 GCMC simulations

### 2.1 Carbon pore models—ideal pores

Adsorption in carbon pores having different shapes (i.e. slit-like, cylindrical, hexagonal and quadratic) is studied. The dimensions of pores were assumed to be essentially the same (of course due to geometry restrictions the volumes of the adsorption space are different).

Figure 1 shows the considered pore geometries and the location of pores in the coordinate system (only the internal walls are shown). Two movies attached to Electronic Supplementary Material and Figs. 1 and 2 were created using the VMD program (Humphrey et al. 1996). The studied structures are placed in the same way (and have the same dimension) in the $z$ direction and have the ends to enable the application of the periodic boundary conditions. The internal wall of each pore is constructed from carbon atoms ($d_{CC} = 0.141$ nm). During creation of quadratic and hexagonal pores the distance between carbon atoms forming the neighboring walls was checked, i.e. it should be larger (or equal to) than $d_{CC}$. If this distance was smaller the atoms were symmetrically deleted. Three carbon layers separated by $\Delta = 0.335$ nm were considered in each wall (plus the internal wall which was defected).

In the $x$ and $y$ directions the dimensions of simulation box were limited by the values of $D_{cyl}$, $H_{slit}$, $H_{quad}$, and $H_{hex}$ (they are collected in Table 1). Those values were selected basing on the diameter of the cylinders given by:

$$D_{cyl} = d_{CC}\{3(n^2 + nm + m^2)\}^{1/2}/\pi \quad (1)$$

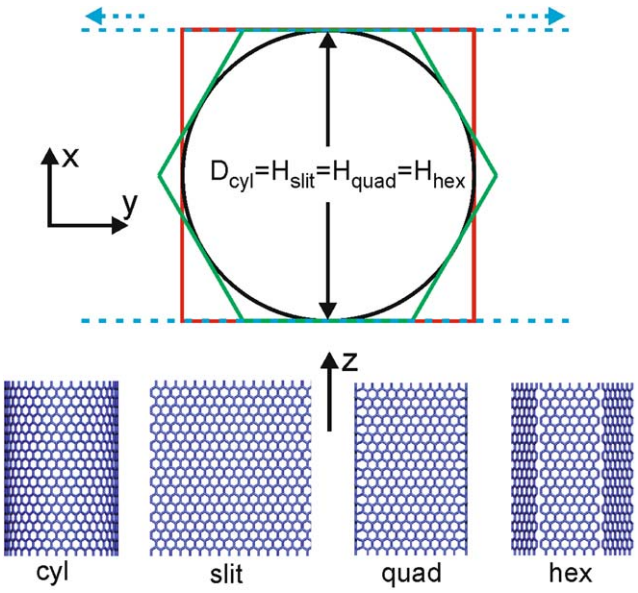


**Fig. 1** The relation between geometric parameters of considered pores (*upper panel*—view from the top) and the side—view of the structure str_3 (Table 1)

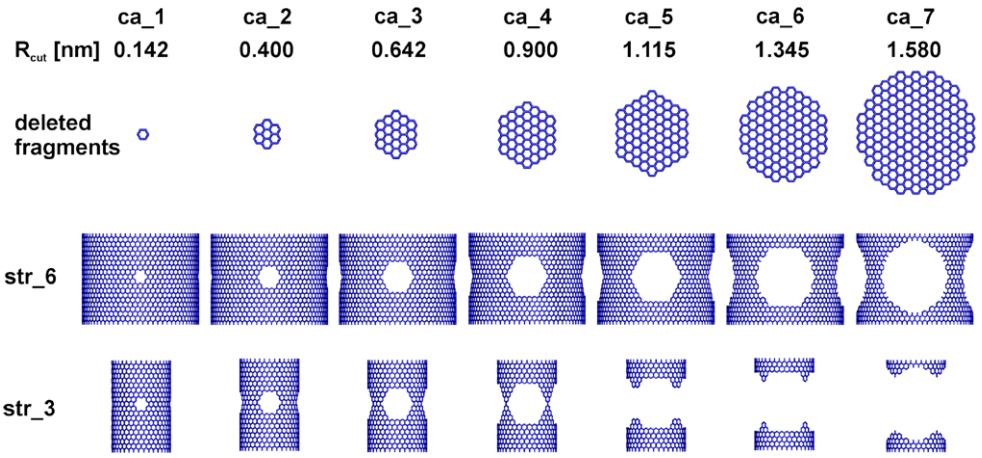


**Fig. 2** The values of the radius of defecting sphere $R_{cut}$, the fragments deleted from the internal carbon walls and the final structures for two of seven considered nanotubes

**Table 1** The parameters characterizing pores. The ideal geometry of the adsorption space is assumed

| | cyl | | slit | quad | hex |
|---|---|---|---|---|---|
| | (n,m) | $D_{cyl}$ [nm] | $H_{slit}$ [nm] | $H_{quad}$ [nm] | $H_{hex}$ [nm] |
| str_1 | (12,0) | | 0.933 | | |
| str_2 | (24,0) | | 1.866 | | |
| str_3 | (36,0) | | 2.798 | | |
| str_4 | (48,0) | | 3.731 | | |
| str_5 | (60,0) | | 4.664 | | |
| str_6 | (72,0) | | 5.597 | | |
| str_7 | (84,0) | | 6.530 | | |

They were chosen to obtain similar structures; therefore, the value of $n$ in $(n, m)$ was changed by 12 for $m = 0$ (we applied the Nanotube Modeller software (JCrystalSoft, USA)). Thus, seven ideal adsorbents (named ca_0) with various widths were considered (Table 1). The defecting of walls produces the pits located at the same place for different structure diameters (see also Fig. 2, ca_1, ..., ca_7). We choose the diameters of pores allowing the occurrence of capillary condensation.

## 2.2 Carbon pore model—pores with defects

The idea of the creation of defects in carbon walls first was proposed by Turner and Quirke (1998) who studied by the GCMC simulation the influence of defected graphite surface on adsorption properties of carbon black toward nitrogen. This idea was also applied by Do et al. who, to introduce the defects, proposed the simple numerical procedure (Brikett and Do 2007; Do and Do 2006) used also in this study. We considered the spheres having the center located inside the six-member carbon ring. In this way two defects were created for slits (each located on opposite wall), four for quadratic and cylindrical pores, and six for hexagonal ones. Next, the values of the radius of the spheres ($R_{cut}$) deleting carbon atoms from each layer were progressively increased (see Fig. 2). In this figure we show the fragments (from slit-like, hexagonal and quadratic pores) deleted by this procedure from sufficiently large pores of the investigated adsorbents (the problem of the overlapping of the adjacent tips). Of course those fragments have different curvature for cylinders, but the differences are not too large. The rise in the value of $R_{cut}$ leads to the rise in the number of deleted carbon atoms and depending on the size of the pore, this can lead to deleting of almost all carbon atoms from inside (str_3—Fig. 2). In such a case all created "holes" join (this situation occurs for ca_5 and larger). However, it does not occur for the case of larger pores and here the independent areas of heterogeneity are still present.

## 2.3 Simulation of Ar adsorption isotherms

For all pores Ar adsorption isotherms were simulated using the Grand Canonical Monte Carlo method. The probabilities of an attempt of the change of the state of the systems *via* displacement, creation and/or annihilation of Ar atom were the same and equal to (1/3). For all pore geometries the length of the simulation box was equal to $L_z = 4.23$ nm. All isotherms were simulated for the temperature of $T = 87$ K. Periodic boundary conditions were applied in one or two directions, depending on pore geometry.

### *2.3.1 Fluid-fluid interactions*

The energy of fluid-fluid (ff) interactions was modeled by the classical Lennard-Jones potential (Frenkel and Smit 1996):

$$U_{ff}(r) = 4\varepsilon_{ff}\left[\left(\frac{\sigma_{ff}}{r}\right)^{12} - \left(\frac{\sigma_{ff}}{r}\right)^{6}\right] \quad (2)$$

using the following values of the parameters: $\sigma_{ff} = 0.3405$ nm, $\varepsilon_{ff}/k_B = 119.8$ K (Do and Do 2005). The potential cut-off was at $r_{cut} = 5\sigma_{ff}$.

### 2.3.2 Solid-fluid interactions

The energy of solid-fluid interactions with the internal layer of a carbon pore was calculated from:

$$U_{sf}^{h} = 4\varepsilon_{sf}\sum_{i=1}^{M}\left[\left(\frac{\sigma_{sf}}{r_i}\right)^{12} - \left(\frac{\sigma_{sf}}{r_i}\right)^{6}\right] \quad (3)$$

where $M$ is the number of carbon atoms forming the wall, $r_i$ is the distance between an adsorbate atom and $i$th carbon atom forming the internal layer. We assumed: $\sigma_{sf} = 0.34025$ nm, $\varepsilon_{sf}/k_B = 57.92$ K (Do and Do 2005).

The solid-fluid interactions with three outer and ideal carbon layers (separated by $\Delta$) were calculated using analytical potential models. The interaction with each layer was calculated by summation for cylindrical, hexagonal and quadratic pores. In the case of the slit-like geometry the infinity walls were taken into account due to the mathematical form of the fluid-solid potential.

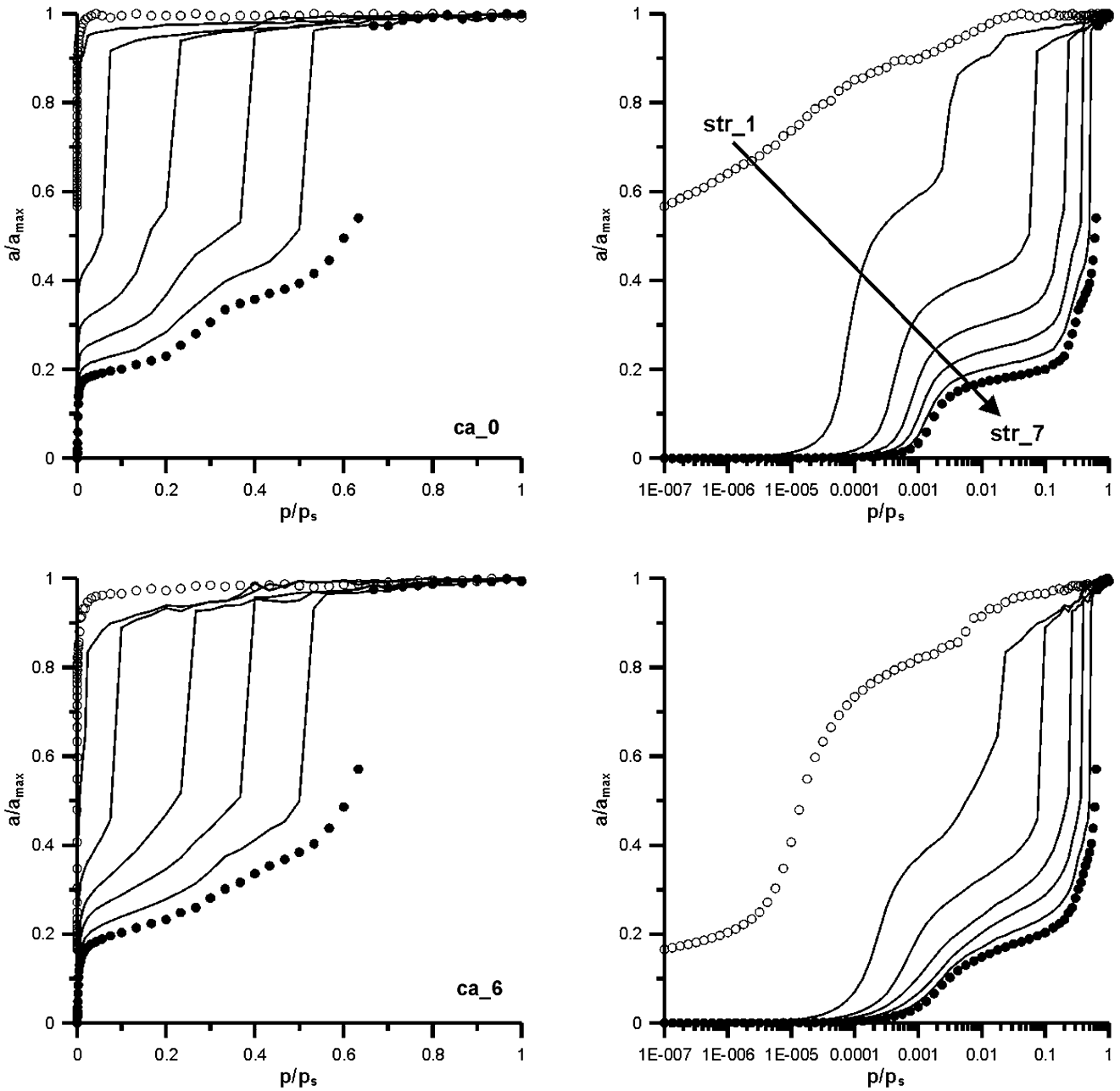


**Fig. 3** GCMC Ar ($T = 87$ K) adsorption isotherms for ideal carbon nanotubes and for tubes with defects

For cylinders (Tanaka et al. 2002):

$$U^a_{\mathrm{sf}}(r) = \pi^2 \rho_{\mathrm{s}} \varepsilon_{\mathrm{sf}} \sigma^2_{\mathrm{sf}} \times \left[ \frac{63}{32} \frac{F\left(-\frac{9}{2}, -\frac{9}{2}, 1, \beta^2\right)}{[R^*(1-\beta^2)]^{10}} - 3 \frac{F\left(-\frac{3}{2}, -\frac{3}{2}, 1, \beta^2\right)}{[R^*(1-\beta^2)]^4} \right] \tag{4}$$

where: $\beta = \frac{r}{R}$, $R^* = \frac{R}{\sigma_{\mathrm{sf}}}$, and $R$ is the tube radius, $r$ is the distance of the argon atom from the tube centre, $\rho_{\mathrm{s}}$ is the density of carbon atoms in the wall (38.2 nm$^{-2}$), $F(a, b, c, z)$ is the four parameter hypergeometric function given by

$$F(a, b, c, z) = 1 + \frac{ab}{c} \cdot z + \frac{1}{2!} \cdot \frac{a(a+1)(b+1)}{c(c+1)} \cdot z^2 + \cdots \tag{5}$$

For slit-like pores we used the potential derived by Steele (1973):

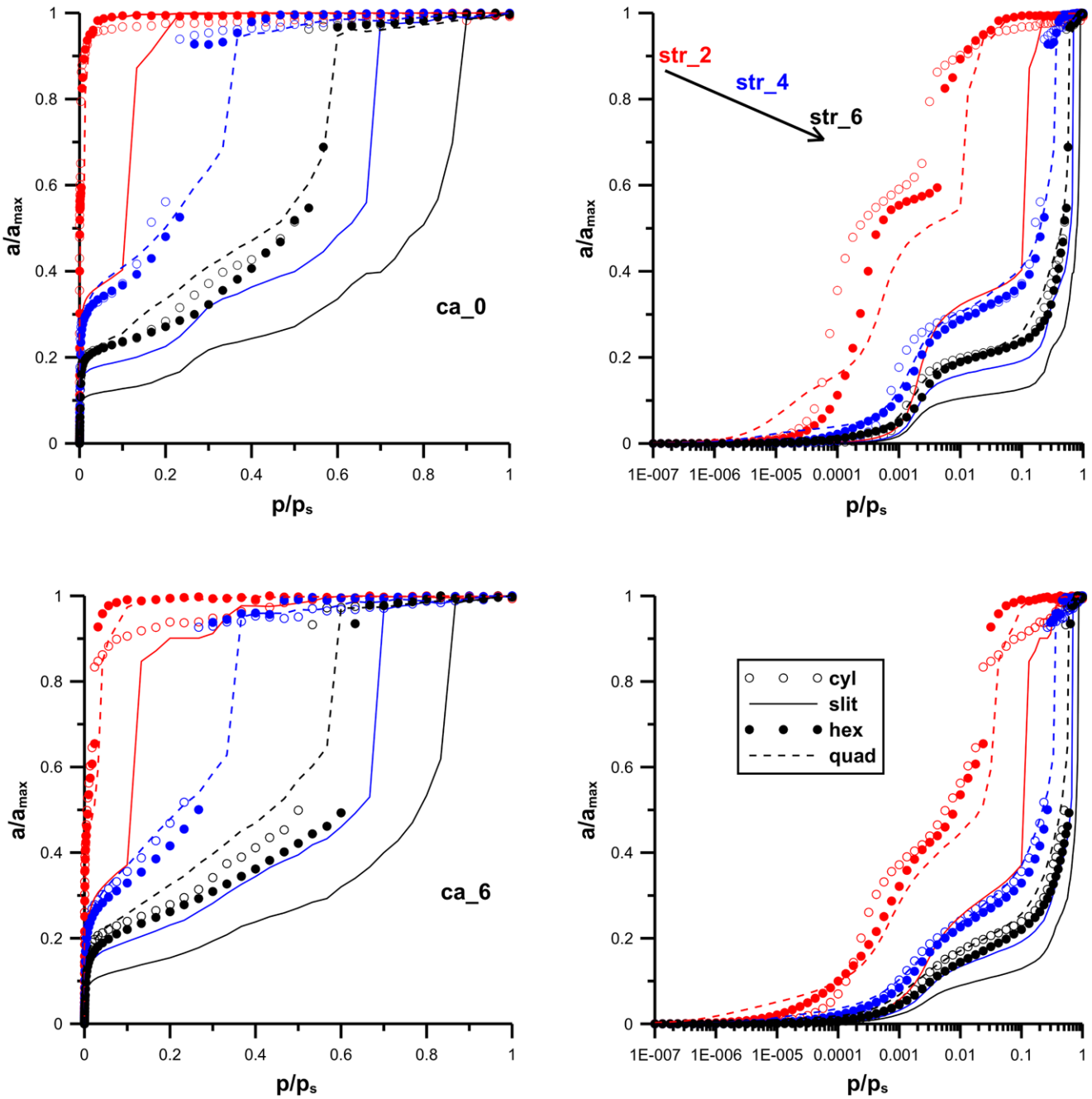


**Fig. 4** The comparison of simulated isotherms for two studied geometries and for ideal and for arbitrarily chosen models with defects

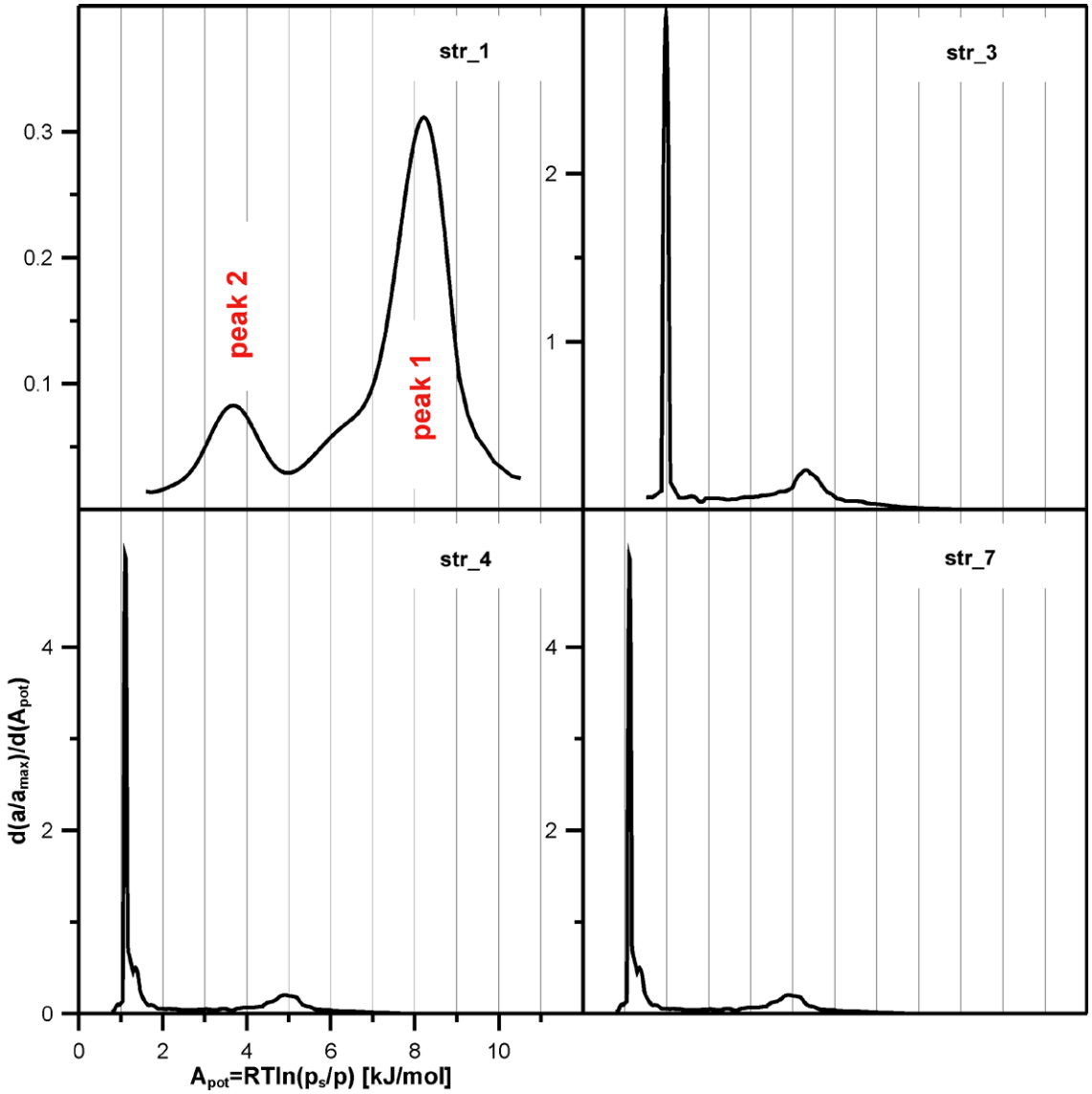


**Fig. 5** The changes in the shapes of APD curves for nanotubes having the same wall defects (ca_3) with the rise in the tube diameter

$$U^{a}_{\mathrm{sf}}(z) = 2\pi\rho_{\mathrm{s}}\varepsilon_{\mathrm{sf}}\sigma^{2}_{\mathrm{sf}} \times \left[\frac{2}{5}\left(\frac{\sigma_{\mathrm{sf}}}{z}\right)^{10} - \left(\frac{\sigma_{\mathrm{sf}}}{z}\right)^{4} - \frac{\sigma^{4}_{\mathrm{sf}}}{3\Delta(z+0.61\Delta)^{3}}\right] \tag{6}$$

where $z$ is the distance of Ar atom from the pore wall.

Quadratic and hexagonal pores were constructed from graphitic carbon layers finite in one direction and infinite in the second. The potential energy of interactions with such a wall is given by Bojan and Steele (1988, 1989):

$$U_{\mathrm{sf}}(y,z) = \frac{1}{2}\pi\rho_{\mathrm{s}}\varepsilon_{\mathrm{sf}}\sigma^{6}_{\mathrm{sf}}[U_{\mathrm{rep}}(y_1,z) - U_{\mathrm{rep}}(y_2,z) - U_{\mathrm{att}}(y_1,z) + U_{\mathrm{att}}(y_2,z)] \tag{7}$$

where:

$$U_{\mathrm{rep}}(y,z) = \frac{\sigma^{6}_{\mathrm{sf}}y}{32p}\left(\frac{128}{5z^{10}} + \frac{64}{5z^{8}p^{2}} + \frac{48}{5z^{6}p^{4}} + \frac{8}{z^{4}p^{6}} + \frac{7}{z^{2}p^{8}}\right) \tag{8}$$

$$U_{att}(y,z) = \frac{y}{p}\left(\frac{2}{z^{4}} + \frac{1}{z^{2}p^{2}}\right) \tag{9}$$

$$p = \sqrt{y^{2}+z^{2}} \tag{10}$$

$$y_1 = -\frac{1}{2}w_{\mathrm{s}} - y \tag{11}$$

$$y_2 = \frac{1}{2}w_{\mathrm{s}} - y \tag{12}$$

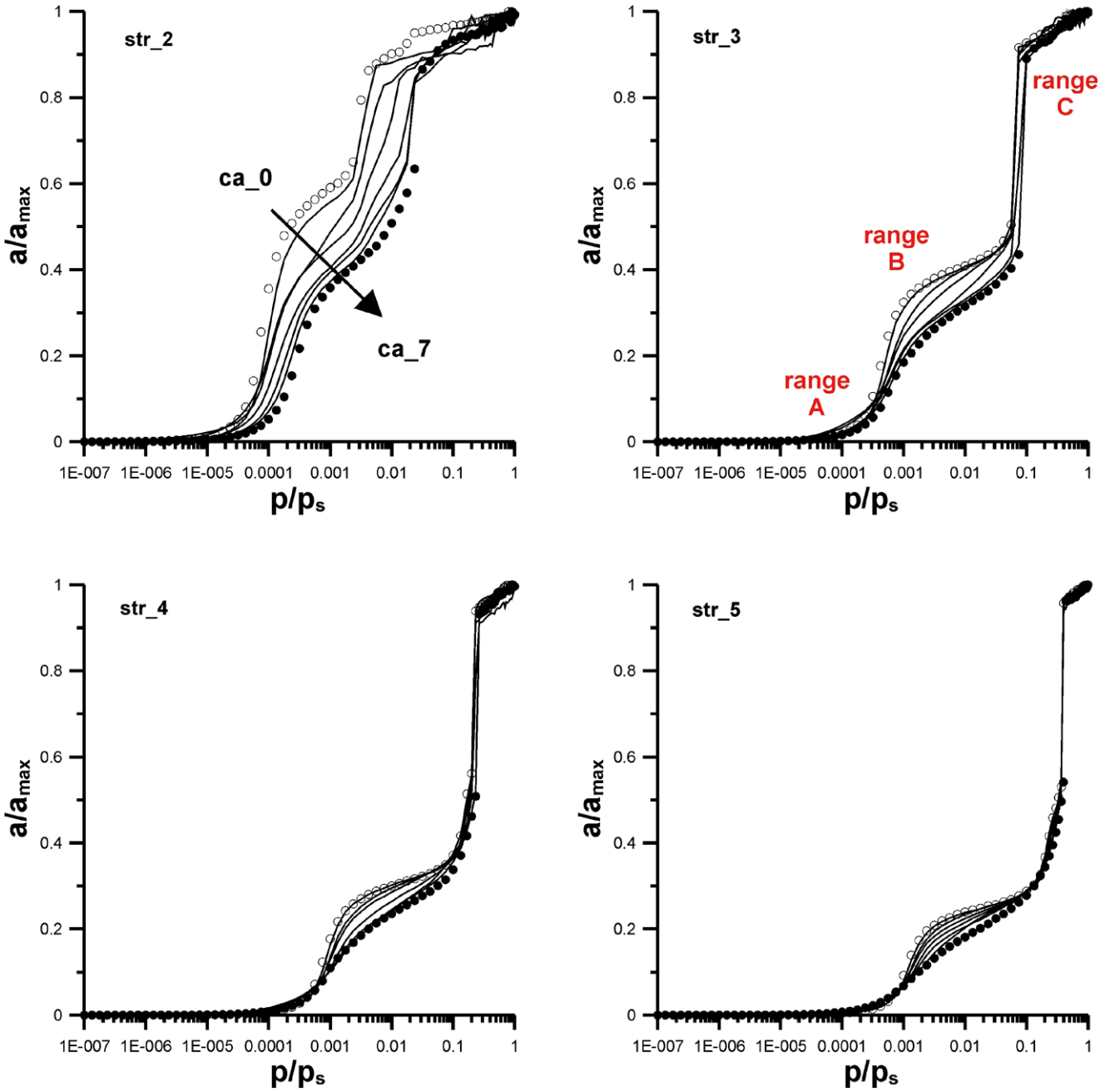


**Fig. 6** The influence of heterogeneity on adsorption isotherms for ideal and nonideal carbon nanotubes. Three considered regions (A, B and C) are shown

and $z$ is the distance of Ar atom from the layer (measured in the direction perpendicular to the layer), $y$ is the distance of Ar atom from the center of the layer (measured in the direction parallel to the layer) and $w_s$ is the diameter of the layer.

## 3 APD and porosity calculation

In order to calculate the APD curve a set of the relative adsorption ($a/a_{max}$) and adsorption potential ($A_{pot} = R_g T \ln(p_s/p)$) data was obtained from the simulated adsorption isotherm. It should be pointed out that we limited the considerations mainly to the range of relative pressures below the capillary condensation. Next, those values were interpolated using spline estimation passes exactly through each data point (cubic constrained). We obtained ca 1000 values of ($a/a_{max}$) vs. $A_{pot}$. Finally, the interpolated curve was differentiated numerically and the application of this procedure guarantees the smooth ($d(a/a_{max})/dA_{pot}$) curve in the range of $A_{pot}$: 3–8 kJ/mol.

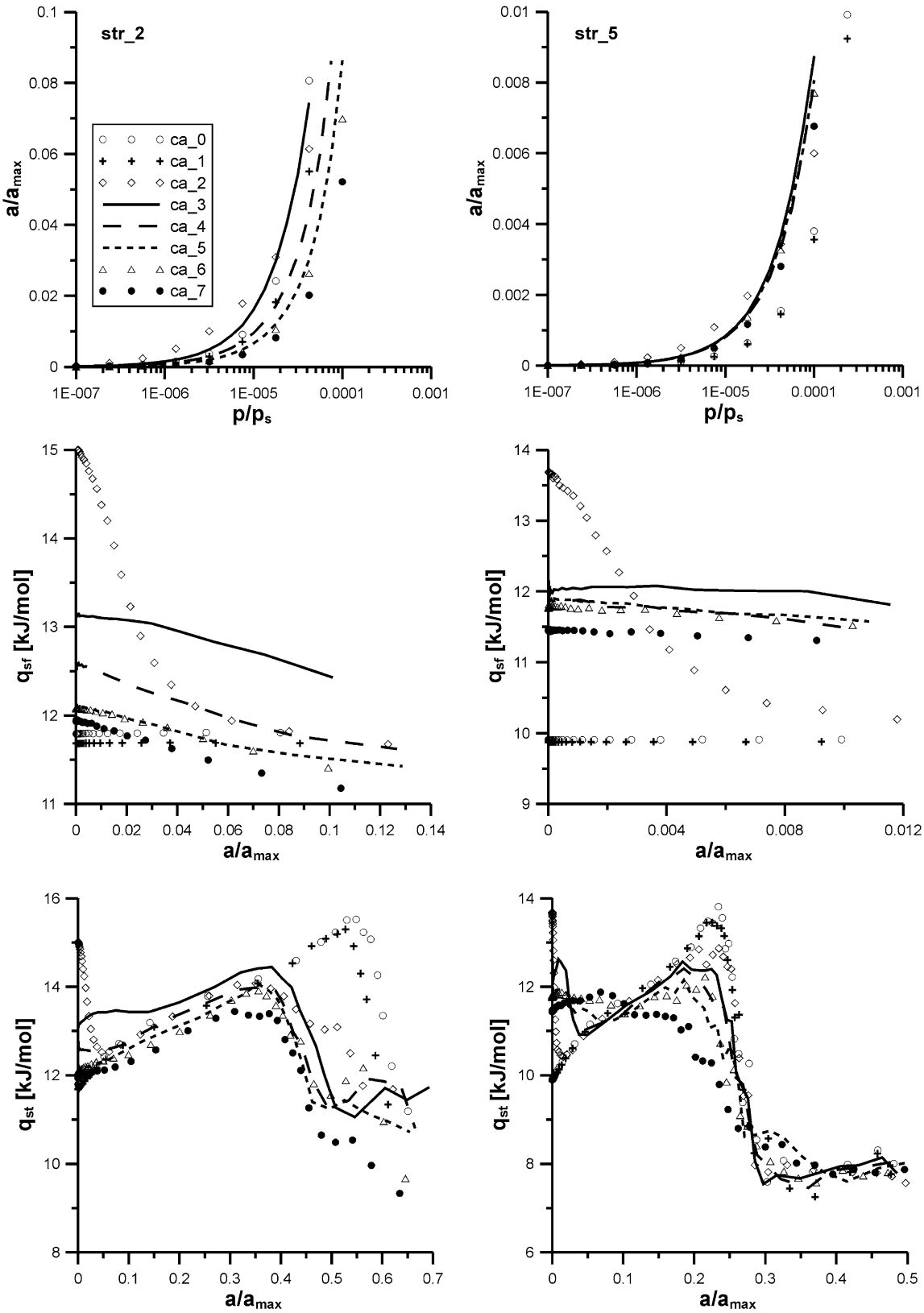


**Fig. 7** *Upper panel*—the comparison of isotherms (from Fig. 6) for ideal and nonideal structures in the range A, *middle panel*—the comparison of the solid—fluid enthalpy of adsorption for this range, *bottom panel*—the differential enthalpy of adsorption in the range up to condensation

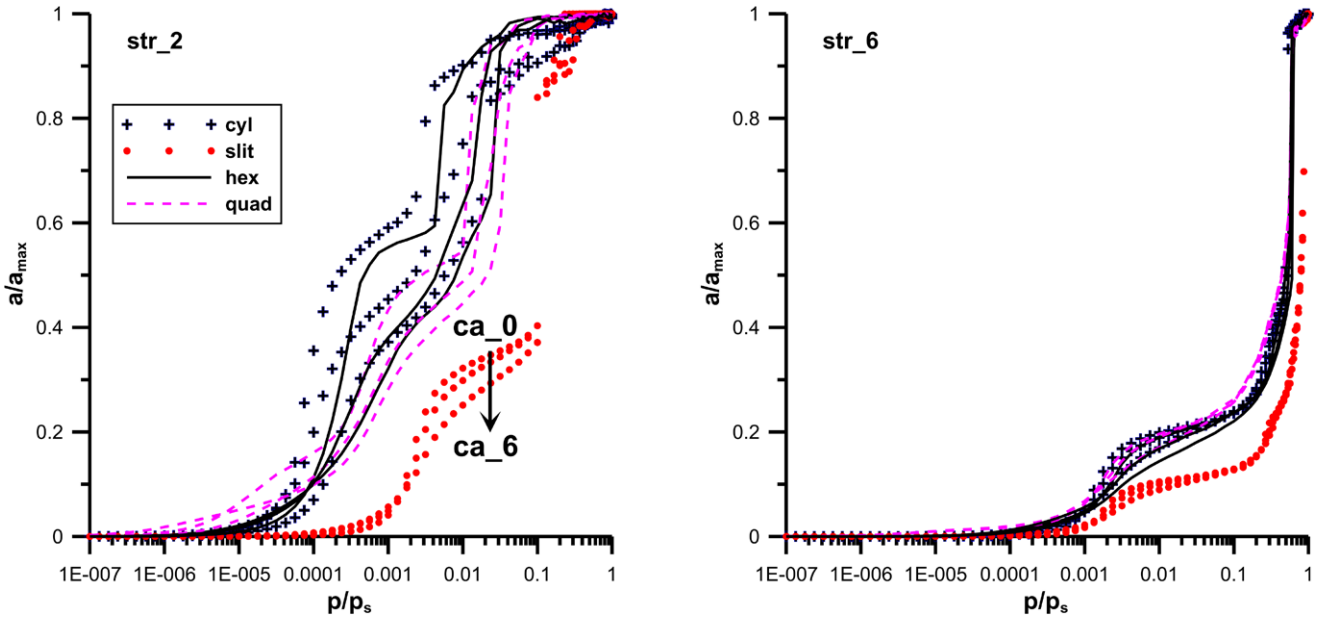


**Fig. 8** The comparison of some isotherms for different geometries in the logarithmic scale

It is interesting to calculate the global parameters characterizing the change of the porosity related to the creation of defects in carbon walls. Therefore, we considered the percentage of deleted carbon atoms from internal carbon layer to their total amount (*% burn-off*). Moreover, the average width was calculated from:

$$width = D_{\mathrm{cyl}}(\equiv H_{\mathrm{slit}}, H_{\mathrm{quad}}, H_{\mathrm{hex}}) + 2\Delta(burn\text{-}off) \qquad (13)$$

We propose this equation, since if $burn\text{-}off = 1$, the width of a pore increases by $2\Delta$. For smaller burn-offs intermediate values of the width are observed.

## 4 Results

Figure 3 shows the comparison of the results of GCMC simulation for ideal carbon nanotubes and tubes with defects. One can observe the change in the shape of isotherms (plotted as the relative adsorption) caused by the creation of the following layers, and the presence of capillary condensation with increasing tube diameter. This effect is obvious and was observed previously (Ohba and Kaneko 2002). Figure 4 shows the comparison of adsorption isotherms for four considered geometries, for three structures and for ideal and nonideal models. One can see that due to the potential energy in pores related to the structure of considered model pores, for hexagons and cylinders similar plots are recorded, and only for slit-like pores the largest differences are seen.

In Fig. 5 the comparison of the APD curves is presented for four tubes having the same defects in internal walls, but differing in the diameter. As one can see usually two groups of peaks are visible. As it was reported many times for different adsorbents (Choma and Jaroniec 1997, 2001; Darmstadt and Roy 2001; Jaroniec and Choma 1986, 1997; Kruk et al. 1998, 1999a, 1999b; McEnaney et al. 1987; Puziy 1995; Terzyk et al. 2007), the peaks at large $A_{\mathrm{pot}}$ values reflect the creation of monolayer, but the second is responsible for the condensation of an adsorbate in pores. The occurrence of those two peaks is recorded almost for all ideal and disturbed adsorbents, moreover with the rise in pore diameter the position and maximum of the first peak change only slightly in comparison with the second peak. Generally, with the rise in the diameter of the tube the condensation peak predominates making the heterogeneity less visible. The same effect occurs for all considered pore geometries and defects. This is the consequence of the potential energy of interactions. The values of this energy are dominated by the energy of fluid-fluid interactions in larger structures, and in this way the behavior of adsorption isotherms is less sensitive for heterogeneity as the tube diameter increases (however, in the monolayer range still the differences are strongly pronounced). Since in this paper we are interested in the effect of heterogeneity, we focus our discussion mainly on the first peak.

Figure 6 shows the influence of heterogeneity on the general behavior of the isotherms for some of the studied nanotubes. Movie 1 from Electronic Supplementary Material shows the comparison of the mechanisms of adsorption for two nanotubes having four different defects in the internal wall. Simulated isotherms can be divided into three regions (A, B and C in Fig. 6). The largest differences in

all ranges ($A$, $B$, $C$) between isotherms simulated for structures with defects are visible for the smallest pore (str_2) due to small contribution of fluid-fluid interactions to adsorption energy. For str_3 and larger pores the influence of heterogeneity on the part of isotherm related to condensation (range C) is not large (for all studied pore geometries, see below), contrary to adsorption in the smallest structure (str_2). As it was expected with the rise in tube diameter the effect of heterogeneity is less pronounced but it is still visible especially in the range B. From the analysis of data shown in Fig. 7 (for str_5 showed previously in Fig. 6) one can observe that in the range A, dominated by the solid-fluid energy, the largest adsorption occurs for structure with defects introduced according to ca_2 scheme, and decreases in the sequence: ca_3, ..., ca_7, ..., ca_0 ∼ ca_1. This is caused by the dimension of the defects, where two opposite effects can be observed, i.e. the widening of the defected area causes the decrease in the energy of solid-fluid interactions, and the rise in energy is observed due to the interaction of adsorbate molecules with the edge carbon atoms. Those

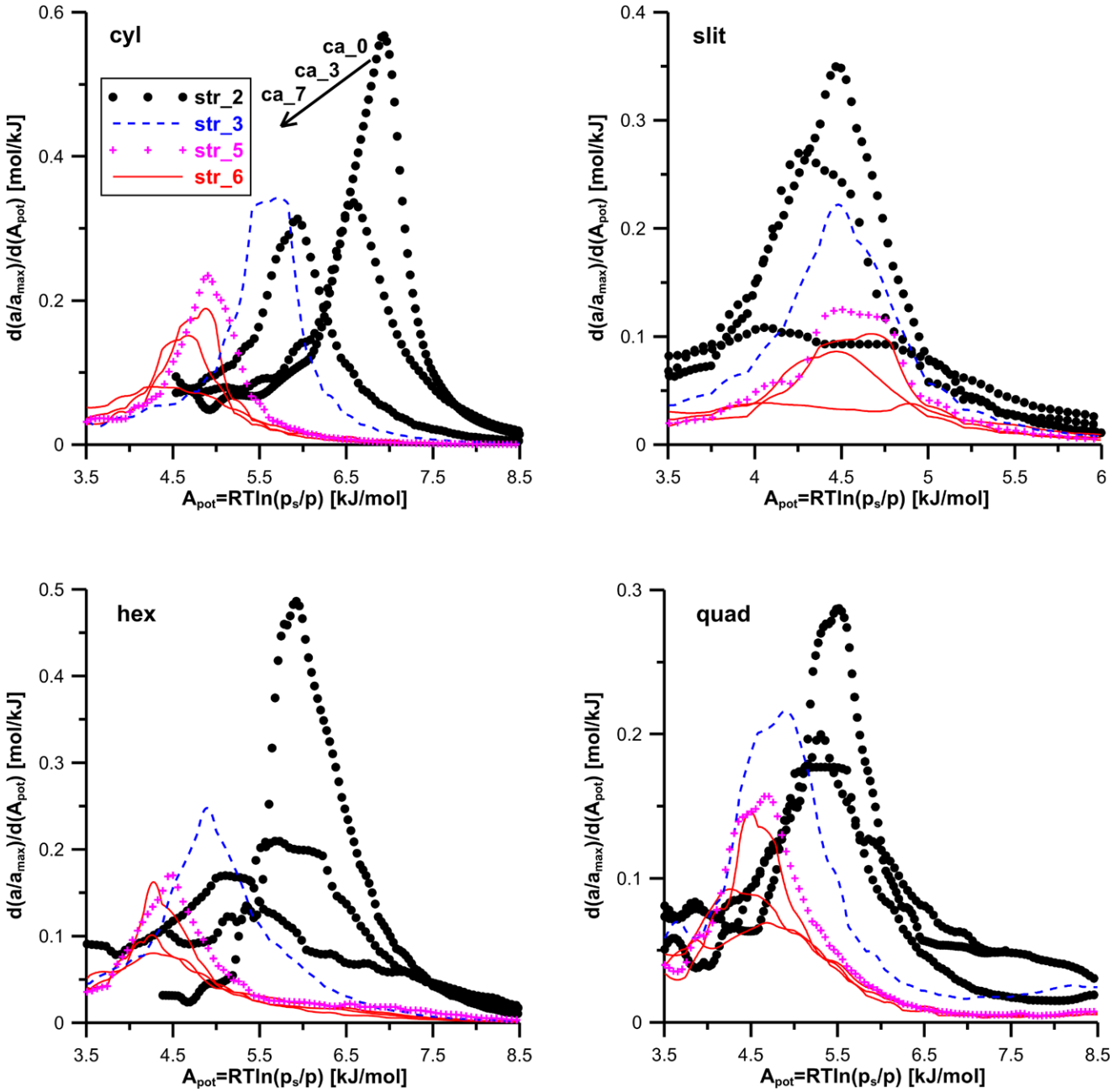


**Fig. 9** The comparison of APD curves for all studied geometries and for ideal and nonideal structures. Note that the influence of defects on APD curves is shown only for str_2 and str_6. For the structures str_3 and str_5 the data for ca_0 are only shown

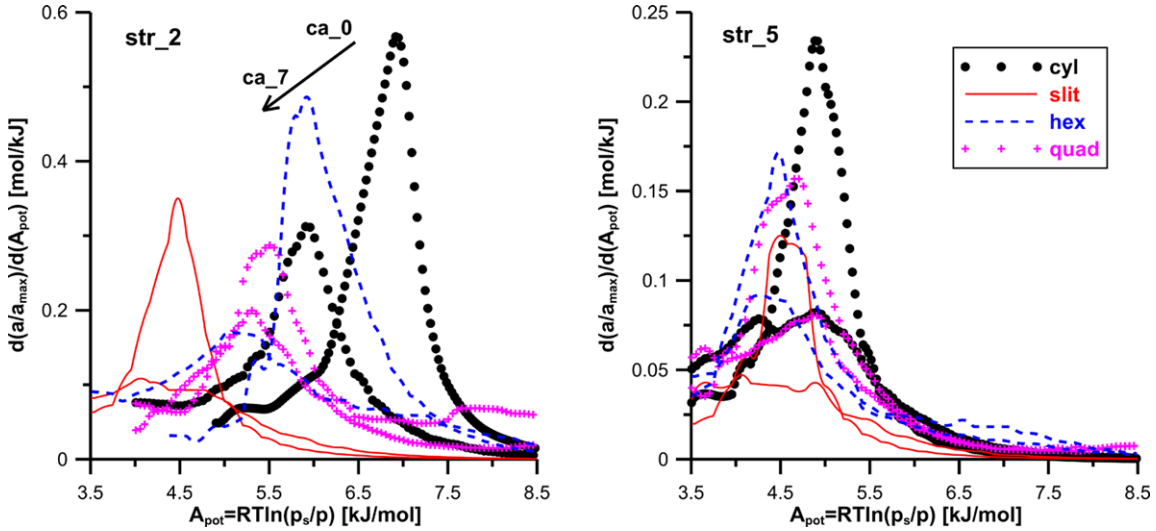


**Fig. 10** APD curves for different studied pore geometries

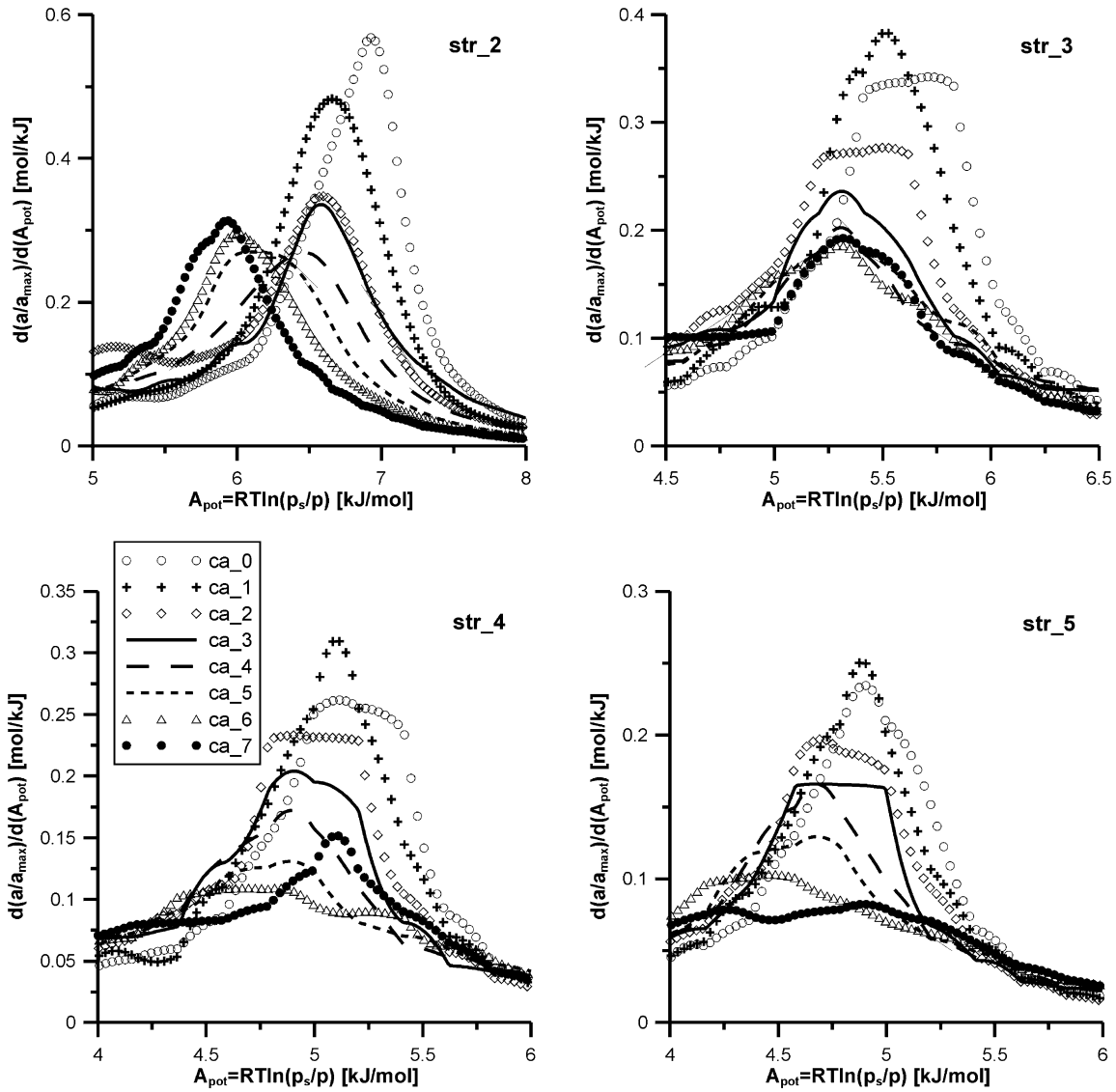


**Fig. 11** The comparison of first peak on the APD curves for ideal and nonideal nanotubes

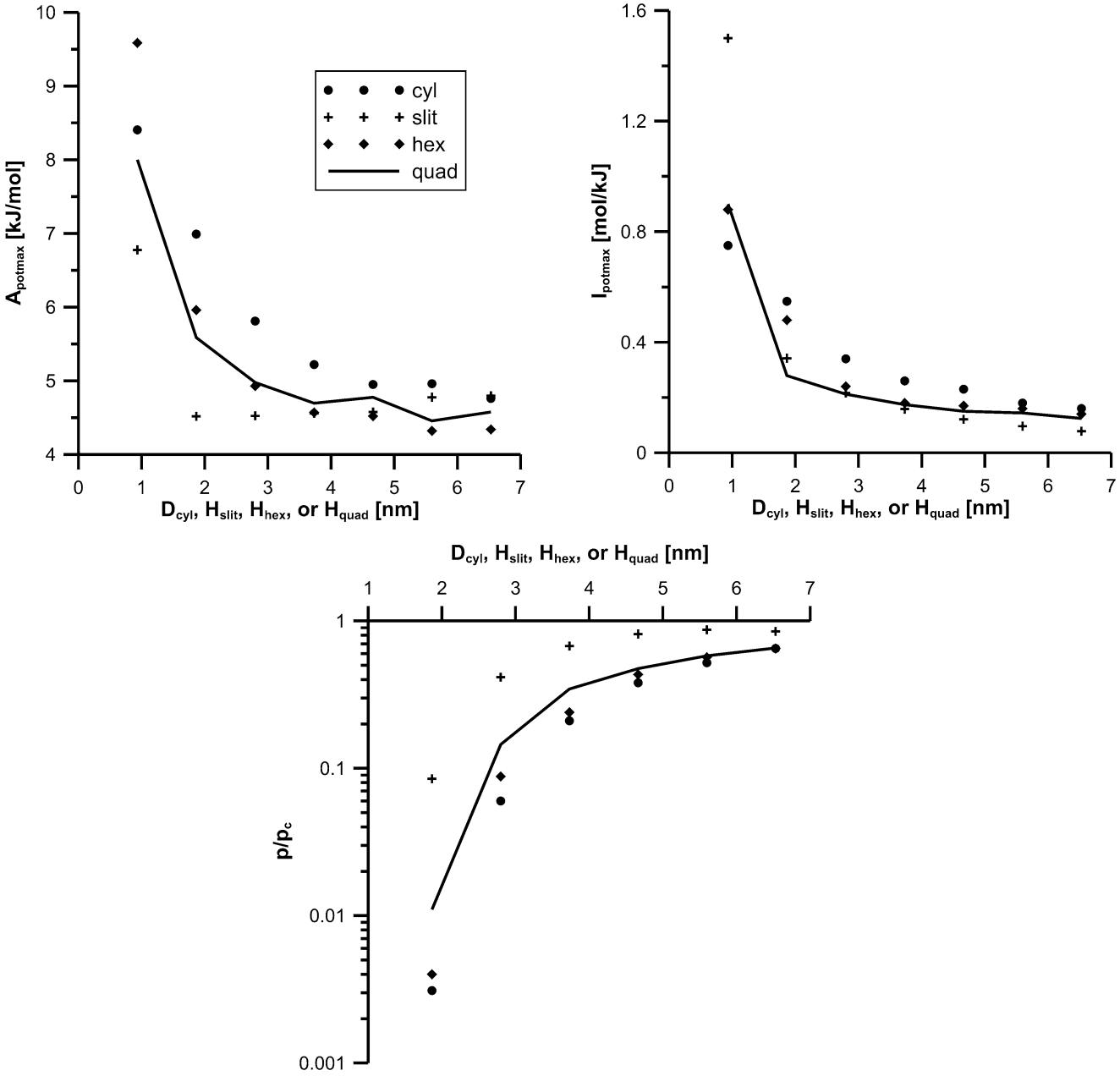


**Fig. 12** The dependence of $A_{\mathrm{potmax}}$, $I_{\mathrm{potmax}}$ and $p/p_{\mathrm{c}}$ on $D_{\mathrm{cyl}}$, $H_{\mathrm{slit}}$, $H_{\mathrm{quad}}$, and $H_{\mathrm{hex}}$ (they are collected in Table 1) for ideal pores (named ca_0)

two effects lead to the most optimal situation for the case of ca_2, having the largest adsorption enthalpy (Fig. 7).

As mentioned above during analysis of the data from Figs. 6 and 7 the most interesting range is the region B where generally adsorption decreases with the rise in the dimension of defects, and adsorption isotherm becomes more linear if plotted in the logarithmic scale. This is caused by the mentioned above two opposite effects, causing the "delay" in creation of monolayer for the most defected structures, moreover this creation is not so strongly pronounced as for the initial structure (see Movie 1). In Fig. 8 we show the results for two structures and for four geometries of the adsorption space. For all shapes of pores in range B similar qualitative behavior is observed (Fig. 8). In the case of slit-like pores the influence of heterogeneity is the smallest in this range, due to smaller adsorption potential and smaller number of defects (see Movie 2).

The comparison of APD curves is presented in Fig. 9 for all studied pore geometries, for ideal pores (str_2, 3, 5 and 6) and for pores with defects (str_2 and 6). Although the amount of defects is sometimes small, the APD curves are very sensitive to pore geometry (cylindrical and hexag-

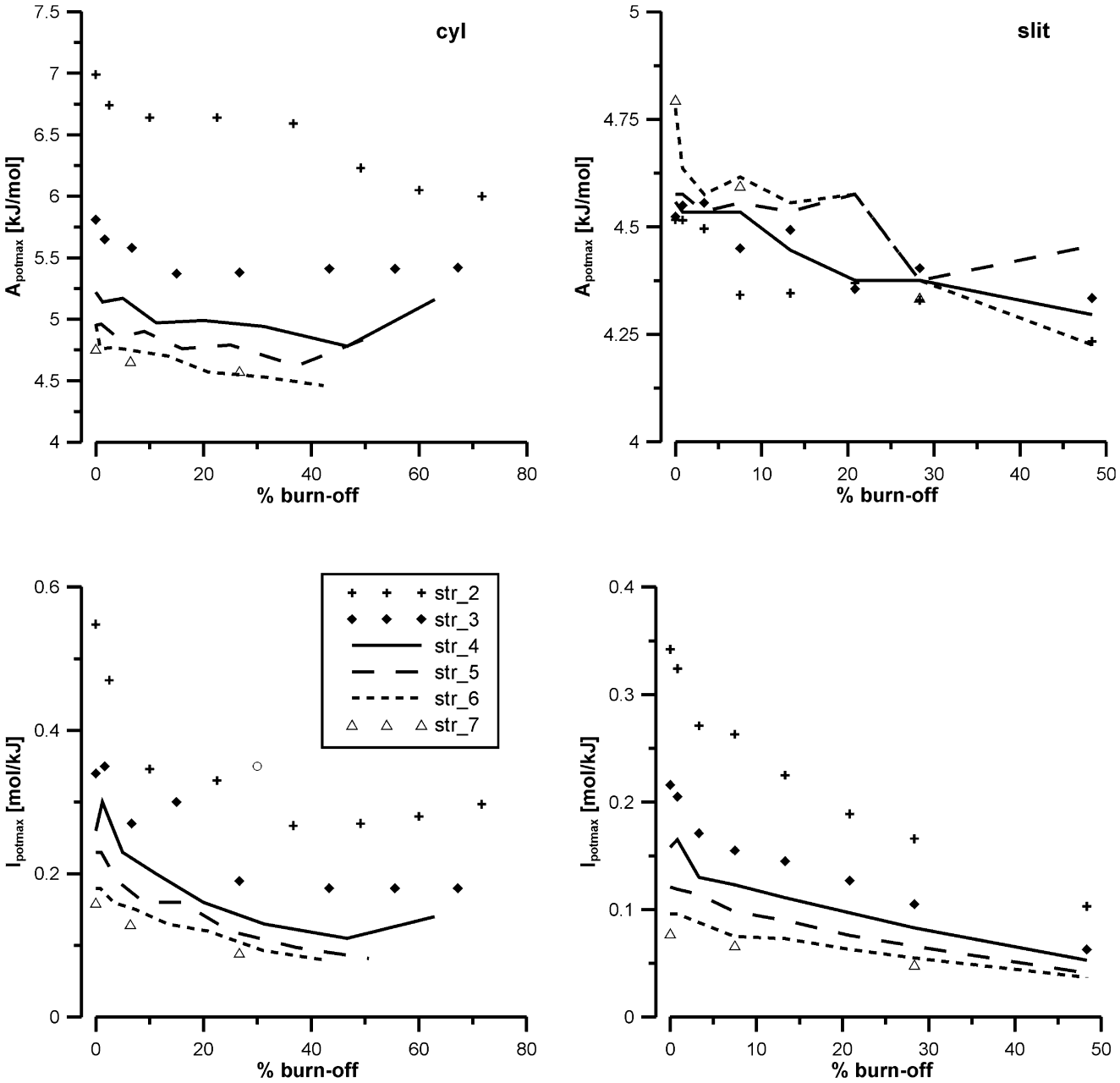


**Fig. 13** The dependence between $A_{potmax}$, $I_{potmax}$ and the burn off for studied structures

onal pores are the most sensitive) as well as to the presence of defects. The rise in the diameter of a pore causes the decrease in intensity of the analysed peak, its flattening, and this peak shifts towards smaller potential value, with exception of slits, where the location of this maximum is practically unchanged. In Fig. 10 the comparison of APDs for small and large pores is shown. One can see, that for pores with small dimensions, where the influence of heterogeneity is large, the location of maxima on APD curve shifts toward smaller potential values in the order: cylindrical, hexagonal, quadratic, slit-like (for initial as well as for structures with defects). For larger diameters smaller differences are observed in location of the maxima. In Fig. 11 we show the influence of heterogeneity on APD curves for cylindrical pores (the comparison for other geometries will be shown as the values of maxima ($A_{potmax}$) of potential and its intensity ($I_{potmax}$) in next figures with different correlations). Some nuances of the first peak are shown in Fig. 11. One can observe the gradual decrease in the intensity, and flattering of this peak with the rise in heterogeneity of the internal wall, and for the smallest nanotubes the shift of the peak toward smaller adsorption potential values (with small increase in

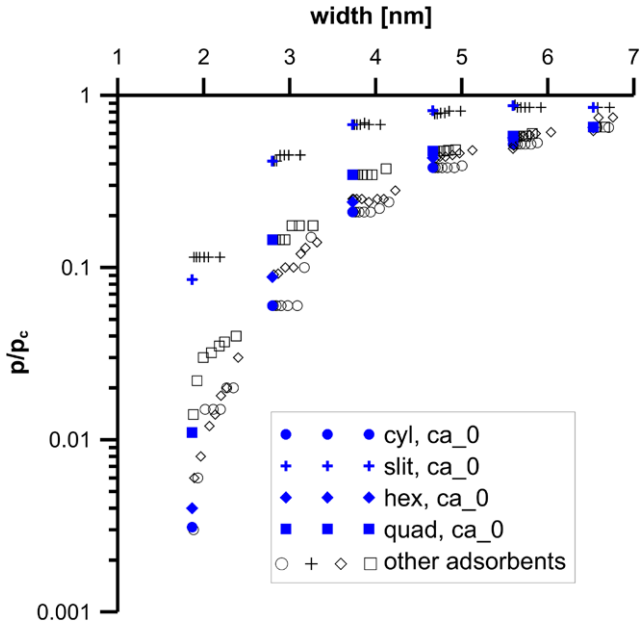


**Fig. 14** The influence of the change in hypothetical average pore widths (see Fig. 13) on the value of $p/p_c$

intensity). Summing up the behaviour of the APD curves with the introduction of heterogeneity changes with the rise in tube diameter since for small tubes we observe the simultaneous changes in both intensity and the location of the peak, while for large ones only the decrease in intensity.

To study the systematic changes in all obtained data we tried to find different correlations that can be useful from experimental point of view. For example, in Fig. 12 we present correlations between $A_{\text{potmax}}$ (and $I_{\text{potmax}}$), the pore filling pressure ($p/p_c$) and the diameter of considered ideal (i.e. ca_0) pores. One can observe very nice recovering of the relation plotted for slit-like pores (Fig. 6 in Kruk et al. (1999b)) on the basis of experimental data. Moreover, obtained plots show that the relation between intensity and the pore diameter should be also observed. For each pore geometry the hyperbolic-like plots occur, and the differences vanish for larger pores with diameter c.a. 5 nm and more. The values of the pore filling pressures show that among studies geometries, for a chosen diameter, condensation is first observed for hexagonal pores, and next for cylinders, quadratic pores and finally for slits. As it was expected for largest pores the differences between pore filling pressures vanish. Figure 13 is particularly interesting, and shows how the % burn-off influences the three considered values (we focus here on the most common geometries i.e. cylinders and slits). For cylindrical pores one should expect that the effect of heterogeneity is strongly pronounced for pores smaller than str_4, i.e. below the diameter of c.a. 4 nm, while for slit-like pores the influence of heterogeneity on the $I_{\text{potmax}}$ values (and not on the $A_{\text{potmax}}$) is strongly marked. In Fig. 14 we show the influence of hypothetical average pore width (see Fig. 13) on the pore filling pressure. One can see that the largest influence of heterogeneity on pore filling pressure is recorded for the smallest pores, as expected. Therefore, in the condensation-approximation-like methods the heterogeneity effect can strongly disturb the relationship between pore width and pore filling pressure.

## 5 Conclusions

The idea of presented study originates from the fundamental papers of Jaroniec et al. We recover their data using molecular simulations moreover we show the comprehensive study of the effect of heterogeneity on the APD curves for pores with different geometries. The results show that APD is very sensitive on pore geometry as well as on heterogeneity. Therefore, this method is excellent supplement of different standard methods of characterization of solid adsorbents.

**Acknowledgements** The authors acknowledge the use of the computer cluster at Poznań Supercomputing and Networking Center and the Information and Communication Technology Center of the Nicolaus Copernicus University (Toruń, Poland). The project was supported by grants: N N204 009934 and N N204 288634.

## References

Bojan, M.J., Steele, W.A.: Computer simulation of physisorption on a heterogeneous surface. Surf. Sci. **199**, L395–L402 (1988)
Bojan, M.J., Steele, W.A.: Computer simulation of physisorbed Kr on a heterogeneous surface. Langmuir **5**, 625–633 (1989)
Brikett, G.R., Do, D.D.: On the physical adsorption of gases on carbon materials from molecular simulation. Adsorption **13**, 407–424 (2007)
Choma, J., Jaroniec, M.: Energetic and structural heterogeneity of synthetic microporous carbons. Langmuir **13**, 1026–1030 (1997)
Choma, J., Jaroniec, M.: A model-independent analysis of nitrogen adsorption isotherms on oxidized active carbons. Colloid Surf. A **189**, 103–111 (2001)
Darmstadt, H., Roy, C.: Comparative investigation of defects on carbon black surfaces by nitrogen adsorption and SIMS. Carbon **39**, 841–848 (2001)
Do, D.D., Do, H.D.: Effects of potential models in the vapor-liquid equilibria and adsorption of simple gases on graphitized thermal carbon black. Fluid Phase Equilib. **236**, 169–177 (2005)
Do, D.D., Do, H.D.: Modeling of adsorption on nongraphitized carbon surface: GCMC simulation studies and comparison with experimental data. J. Phys. Chem. B. **110**, 17531–17538 (2006)
Frenkel, D., Smit, B.: Understanding Molecular Simulation. Academic Press, San Diego (1996)
Gil, A.: Analysis of the micropore structure of various microporous materials from nitrogen adsorption at 77 K. Adsorption **4**, 197–206 (1998)
Humphrey, W., Dalke, A., Schulten, K.: VMD: visual molecular dynamics. J. Mol. Graph. **14**, 33–38 (1996)
Jaroniec, M., Choma, J.: Characterisation of heterogeneity of activated carbons by utilizing the benzene adsorption data. Mater. Chem. Phys. **15**, 521–536 (1986)
Jaroniec, M., Choma, J.: Characterization of geometrical and energetic heterogeneities of active carbons by using sorption measurements. Stud. Surf. Sci. Catal. **104**, 715–744 (1997)

Korili, S.A., Gil, A.: On the application of various methods to evaluate the microporous properties of activated carbons. Adsorption **7**, 249–264 (2001)

Kruk, M., Jaroniec, M., Choma, J.: Comparative analysis of simple and advanced sorption methods for assessment of microporosity in activated carbons. Carbon **36**, 1447–1458 (1998)

Kruk, M., Li, Z., Jaroniec, M., Betz, W.R.: Nitrogen adsorption study of surface properties of graphitized carbon blacks. Langmuir **15**, 1435–1441 (1999a)

Kruk, M., Jaroniec, M., Gadkaree, K.P.: Determination of the specific surface area and the pore size of microporous carbons from adsorption potential distributions. Langmuir **15**, 1442–1448 (1999b)

McEnaney, B., Mays, T.J., Causton, P.D.: Heterogeneous adsorption on microporous carbons. Langmuir **3**, 695–699 (1987)

Ohba, T., Kaneko, K.: Internal surface area evaluation of carbon nanotube with GCMC simulation-assisted $N_2$ adsorption. J. Phys. Chem. B **106**, 7171–7176 (2002)

Puziy, A.M.: Heterogeneity of synthetic active carbons. Langmuir **11**, 543–546 (1995)

Steele, W.A.: The physical interaction of gases with crystalline solids. I. Gas-solid energies and properties of isolated adsorbed atoms. Surf. Sci. **36**, 317–352 (1973)

Tanaka, H., El-Merraoui, M., Steele, W.A., Kaneko, K.: Methane adsorption on single-walled carbon nanotube: a density functional theory model. Chem. Phys. Lett. **352**, 334–341 (2002)

Terzyk, A.P., Furmaniak, S., Gauden, P.A., Harris, P.J.F., Włoch, J., Kowalczyk, P.: Hyper-parallel tempering Monte Carlo simulations of Ar adsorption in new models of microporous non-graphitizing activated carbon: effect of microporosity. J. Phys. Condens. Matter **19**, 406208-1–17 (2007)

Timofeev, D.P.: About the characterisation of microporous structure of activated carbons. Zh. Fiz. Khim. **48**, 1625–1627 (1974) (in Russian)

Turner, A.R., Quirke, N.: A grand canonical Monte Carlo study of adsorption on graphitic surfaces with defects. Carbon **36**, 1439–1446 (1998)